# Direct Spectroscopic Observation of Closed-Shell Singlet, Open-Shell Singlet, and Triplet *p*-Biphenylyloxenium Ion

Ming-De Li,[†,§] Patrick J. Hanway,[‡,§] Toshia R. Albright,[‡] Arthur H. Winter,*,[‡] and David Lee Phillips*,[†]

[†]Department of Chemistry, University of Hong Kong, Pokfulam Road, Hong Kong S.A.R., P.R. China
[‡]Department of Chemistry, Iowa State University, 2101d Hach Hall, Ames, Iowa 50011, United States

S *Supporting Information*

ABSTRACT: The photophysics and photochemistry of *p*-biphenylyl hydroxylamine hydrochloride was studied using laser flash photolysis ranging from the femtosecond to the microsecond time scale. The singlet excited state of this photoprecursor is formed within 350 fs and partitions into three different transients that are assigned to the *p*-biphenyloxy radical, the open-shell singlet *p*-biphenylyloxenium ion, and the triplet *p*-biphenylyloxenium ion, having lifetimes of 40 μs, 45 ps, and 1.6 ns, respectively, in CH_3CN. The open-shell singlet *p*-biphenylyloxenium ion predominantly undergoes internal conversion to produce the closed-shell singlet *p*-biphenylyloxenium ion, which has a lifetime of 5−20 ns. The longer-lived radical is unambiguously assigned by nanosecond time-resolved resonance Raman (ns-TR^3) spectroscopy, and the assignment of the short-lived singlet and triplet oxenium ion transient absorptions are supported by matching time-dependent density functional theory (TD-DFT) predictions of the absorptions of these species, as well as by product studies that implicate the intermediacy of charged electrophilic intermediates. Product studies from photolysis give *p*-biphenylol as the major product and a chloride adduct as the major product when NaCl is added as a trap. Thermolysis studies give *p*-biphenylol as a major product, as well as water, ammonium, and chloro adducts. These studies provide a rare direct look at a discrete oxenium ion intermediate and the first detection of open-shell singlet and triplet configurations of an oxenium ion, as well as providing an intriguing example of the importance of excited state dynamics in governing the electronic state population of reactive intermediates.
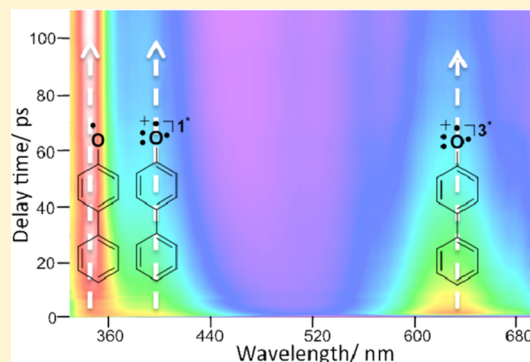
1. INTRODUCTION

Oxenium ions are high-energy reactive intermediates of formula R−O$^+$. These species are isoelectronic to the more familiar nitrene family of intermediates, but, unlike nitrenes, oxenium ions bear a formally positive charge on a highly electronegative hypovalent oxygen atom. In spite of their unusual structure, these intermediates are important in a number of synthetic *umpolung* reactions as well as in biological processes.[1−4] Numerous alkane and phenol oxidations are thought to involve the intermediacy of oxenium ions,[5−7] and oxenium ions are particularly common intermediates in copper and hypervalent iodine-mediated oxidation reactions.[8,9] For example, aryloxenium ions are proposed intermediates in the industrial production of poly(phenyl)ether (PPE),[10−12] a thermoplastic derived from phenol. Additionally, certain enzymes oxidize phenols to quinones through mechanisms that are thought to involve the intermediacy of discrete oxenium ions.[13] While oxenium ions are short-lived in solution, simple oxenium ions have also been detected as persistent species in the interstellar medium,[14,15] and similar to carbenes and nitrenes, they can be stabilized by transition metals, making them an interesting class of ligands.[16]

In spite of their importance to such a diversity of chemists, oxenium ions are poorly understood. A problem that has

hindered a better understanding of oxenium ions has been the lack of general methods to photogenerate these species that would allow them to be directly detected in order to study their reactivities, lifetimes, spectroscopic signatures, and electronic configurations. Studies of related intermediates (carbenes, nitrenes, nitrenium ions) have benefited tremendously from the ability to photogenerate these species from established precursors (azides, azirines, etc.).[17−21] In contrast, there have been few good ways to generate oxenium ions photochemically. These ions have been suggested as intermediates from mixtures from multiphoton ionization studies and from mass spectrometry ion fragmentations.[22−25] However, the development of a robust single photon precursor to this species has proven to be difficult.

Some progress toward general photochemical precursors to oxenium ions has been made, and two discrete oxenium ions have recently been directly detected by laser flash photolysis (LFP).[4,26] In an important paper, Novak and Platz were the first to report the detection of an oxenium ion (the 4′-methyl-4-biphenylyloxenium ion), which was generated from the photolysis of the 4-(4-methylphenyl)-4-acetoxy cyclohexadie-

noyl derivative.[26] See Scheme 1. More recently, we observed the parent phenyloxenium ion as a photoproduct of the phenyl

Scheme 1. Two Prior Studies That Have Detected Discrete Oxenium Ions by LFP,[4,26] and an Overview of This Work
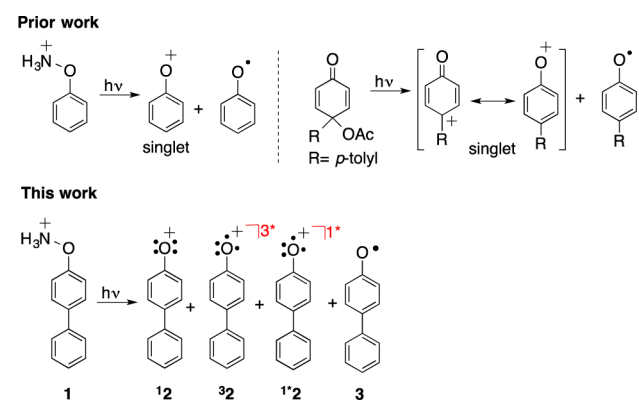
hydroxylamine tetrafluoroborate salt.[27] In addition to a concomitant homolytic process, this hydroxylamine salt undergoes heterolytic scission of the O−N bond to lead to the formation of the singlet phenyloxenium ion and neutral ammonia.[4] Both the detected oxenium ions were seen in their closed-shell singlet ground states.

The possible use of protonated hydroxylamines as photoprecursors to oxenium ions is an intriguing one. These photoprecursors offer a few advantages. First, they are easy to prepare synthetically. Second, they are positively charged rather than neutral and eject a neutral leaving group (ammonia). In principle, a positively charged precursor allows the photolysis to generate oxenium ions in solvents that are nonionizing. In contrast, uncharged precursors require ionizing solvents because they generate an ion pair starting from a neutral species. Finally, they are not, in principle, restricted to generating certain oxenium ion structures.

To test the scope of this photoprecursor, we synthesized the *p*-biphenyl-hydroxylamine hydrochloride salt, which we anticipated could lead to the *p*-biphenylyloxenium ion and allow comparisons to the neutral photoprecursor studied by Novak and Platz.[26] We are pleased to report a combined femtosecond transient absorption (fs-TA), nanosecond transient absorption (ns-TA), and nanosecond time-resolved resonance Raman (ns-TR³) spectroscopic investigation of the photophysics and photochemistry of compound **1** to directly observe the formation of the open-shell singlet *p*-biphenyloxenium ion, the closed-shell singlet state *p*-biphenyloxeniumion, the triplet state *p*-biphenyloxeniumion, and *p*-biphenyloxy radical intermediates after ultraviolet photoexcitation in MeCN solution. To our knowledge this is the first direct detection of an open-shell singlet or a triplet state of an oxenium ion in solution using LFP.

2. EXPERIMENTAL AND COMPUTATIONAL METHODS

The precursor sample compound for the photochemistry and time-resolved spectroscopy experiments was synthesized from a modification of a known procedure of aryloxyamines in 2001.[27,28] See Supporting Information for synthetic procedures. Spectroscopic grade acetonitrile (MeCN) was used to prepare sample solutions for use in the time-resolved spectroscopy experiments.

2.1. Femtosecond Transient Absorption (fs-TA) Experiment. The fs-TA experiments were done by employing an experimental setup and methods detailed previously,[29] and only a brief description is provided here. Fs-TA measurements were done using a femtosecond regenerative amplified Ti:sapphire laser system in which the amplifier was seeded with the 120 fs laser pulses from an oscillator laser system. The laser probe pulse was produced by utilizing ∼5% of the amplified 800 nm laser pulses to generate a white-light continuum (350−800 nm) in a CaF₂ crystal, and then this probe beam was split into two parts before traversing the sample. One probe laser beam goes through the sample while the other probe laser beam goes to the reference spectrometer in order to monitor the fluctuations in the probe beam intensity. For the experiments discussed in this work, a 10 mL solution was flowed through a 2 mm path-length cuvette. This flowing sample was then excited by a 267 nm pump laser beam. An absorbance of 1 at 267 nm was used for the sample solutions for the fs-TA experiments in order to maintain the same number of photons being absorbed for the same irradiating conditions for the samples.

2.2. Nanosecond Transient Absorption (ns-TA) Experiment. The ns-TA experiments: Nanosecond time-resolved transient absorption (ns-TA) measurements were carried out with an LP920 laser flash spectrometer provided by Edinburgh Instruments Ltd. The probe light source is a 450 W ozone-free Xe arc lamp with 10 Hz to single shot operation versatile sample chamber with integral controller, high speed pump and probe port shutters, sample holder, filter holders, which produces a continuous spectrum between 150 to 2600 nm. Measurements of the ns-TA spectra were performed according to the following procedure. The fresh sample solutions were excited by a Q-switched Nd:YAG laser (fourth harmonic line at λ = 266 nm). The probe light from a pulsed xenon arc lamp was passed through various optical elements, samples, and a monochromator before being detected by a fast photomultiplier tube and recorded with a TDS 3012C digital signal analyzer. In the kinetics mode, a photomultiplier detector or InGaAs PIN detector was used and the transient signal acquired using a fast, high-resolution oscilloscope. In the spectral mode an array detector was fitted to the spectrograph exit port to measure a full range of wavelengths simultaneously. Unless specified otherwise, the ns-TA experiments were performed in air-saturated solutions, and the sample solutions were made up to have an absorbance of 1 at 266 nm.

2.3. Nanosecond Time-Resolved Resonance Raman (ns-TR³) Experiments. The ns-TR³ experiments were done by employing an experimental setup and methods detailed previously,[30,31] and only a brief account is provided here. The fourth harmonic of a Nd:YAG nanosecond pulsed laser supplied the 266 nm pump wavelength, and the 341.5 nm probe wavelength came from the second Stokes hydrogen Raman-shifted laser line produced from the fourth harmonic of a second Nd:YAG laser). The pump pulse photoexcited the sample to start the photochemical processes, and the probe pulse monitored the sample and the intermediate species formed. The laser beams were lightly focused and lined up so that they merged together onto a flowing sample. A pulse delay generator was utilized to electronically set the time delay between the pump and probe laser pulses. The Raman scattered signal was collected using a backscattering geometry and observed by a liquid nitrogen-cooled charge-coupled device (CCD) detector. The ns-TR³ spectra shown here were found from subtraction of an appropriately scaled probe-before-pump spectrum from the correlated pump−probe resonance Raman spectrum to mostly get rid of nontransient bands. The Raman bands of MeCN were used to calibrate the Raman shifts with an estimated uncertainty of 5 cm⁻¹. The sample concentrations in ns-TR³ were ∼5 × 10⁻⁴ M.

2.4. Product Studies. Photolysis studies were performed by the addition of 5 mg 4-biphenylyl hydroxylamine hydrochloride **1** to 3 mL of solvent. This solution was then degassed and photolyzed for 1 h in a Rayonet photoreactor. Thermolysis studies were performed by refluxing 10 mg of the precursor compound **1** in 6 mL solvent for 1 h after degassing the solution.

2.5. Density Functional Theory (DFT) Calculations. DFT calculations were performed by employing the (U)B3LYP method with a 6-311G(d,p) basis set. The Raman spectra were found from computing the Raman intensities from transition polarizabilities computed by numerical differentiation, with an assumed zero excitation frequency. A Lorentzian function with a 15 cm⁻¹ bandwidth

for the vibrational frequencies and a frequency scaling factor of 0.974 was used in the comparison of the calculated results with the experimental spectra.[32] TD-DFT was used to calculate the excitation energies and oscillator strengths, the simulation of UV−vis spectra of selected intermediates and excited state were obtained from (U)B3LYP DFT calculations employing a 6-311G(2d,p) basis set in PCM solvent mode. TD-B3LYP has performed well for predicting the absorptions of the parent phenyloxenium ion[4] as well as related species, arylnitrenium ions.[20] No imaginary frequency modes were observed at the stationary states of the optimized structures. All of the calculations were done using the Gaussian 09 program suite.[33]

3. RESULTS AND DISCUSSION

3.1. Femtosecond and Nanosecond Laser Flash Photolysis (LFP) Investigation of p-Biphenylylhydroxyl-amine Hydrochloride 1.
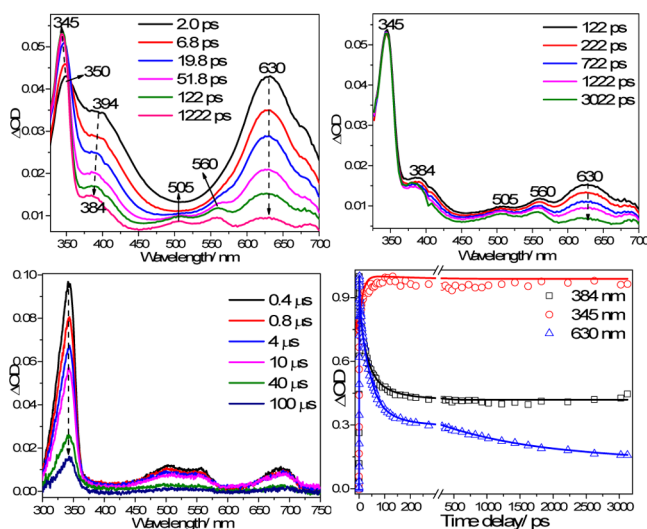Figure 1 shows the evolution of the

Figure 1. TA spectra of species produced in MeCN acquired after 266 nm irradiation of the precursor compound **1** (Top left) LFP from 2 to 122 ps. (Top right) LFP from 122 to 3022 ps. (Bottom left) Nanosecond-TA spectra from 0.4 to 100 μs. (Bottom right) Kinetics of the characteristic fs-TA absorption bands observed at 345, 384, and 630 nm for the fs-TA spectra observed after 266 nm photoexcitation of **1** in MeCN. See text for more details.

transient absorption of the photoprecursor in acetonitrile from 2 to 3022 ps. Immediately after the laser pulse, a broad transient absorption with maxima at 350, 394, and 630 nm

emerges. This transient can be assigned to the first excited singlet state (S_1) of the photoprecursor after 267 nm excitation, which grows in with a time constant of 350 fs. As the maximum absorption at around 630 nm and the shoulder absorption at around 394 nm quickly drop off, a sharp absorption at short wavelength grows in and undergoes a hypsochromic shift from 350 to 345 nm. After 200 ps, the transient absorption at 345 and 382 nm reaches a plateau until 3000 ps. This 345 nm transient can still be seen in the nanosecond transient absorption experiments and decays over ∼39 μs. This transient can be definitively assigned to the p-biphenyloxy radical as seen by ns-TR[3] experiments (described below). However, the transient absorption at 630 nm still decays by a slow process compared to the fast decay process before 200 ps. In addition, a shoulder peak appears at 560 nm which is accompanied by the fast decay of 630 nm.

The fast disappearance of the 630 and 394 nm bands, which can be attributed to S_1 of the photoprecursor, is associated with the appearance of several new transient species. In addition to the radical absorption at a short wavelength described above, two additional transient species are seen. One intermediate, also absorbing at 630 nm, decays over ∼42 ps. A second transient, observed as a peak at ∼394 nm, decays over ∼49 ps. Given the error associated with fitting kinetics of strongly overlapping species, these two absorptions very likely correspond to the same species and the decay waveforms (Figure 2) appear very strongly correlated. A slower decaying transient, also absorbing ∼630 nm, decays with a lifetime of 1.6 ns. On the basis of TD-DFT computations of the UV−vis spectra and trapping studies, we assign the transients absorbing at 630 and 394 nm ($τ ∼ 45$ ps) to the open-shell singlet oxenium ion, and the longer-lived transient ($τ ≈ 1.6$ ns) at 630 nm to the triplet oxenium ion. After 122 ps, the 394 nm transient absorption undergoes a hypsochromic shift from 394 to 384 nm associated with a new species that decays so little over 3000 ps that it is difficult to obtain a good kinetic fit, but approximate fits give a time constant of ∼5 ns. In contrast to the radical absorption, which we observe in the nanosecond LFP experiments, this transient is not detected in the nanosecond LFP experiments. Thus, the lifetime of this final transient must be between 3 and 20 ns (our temporal "blindspot" between the femtosecond and nanosecond LFP setups). We assign this transient absorbing ∼384 nm ($τ ≈ 5$ ns) to the ground-state closed-shell singlet oxenium ion (described below).
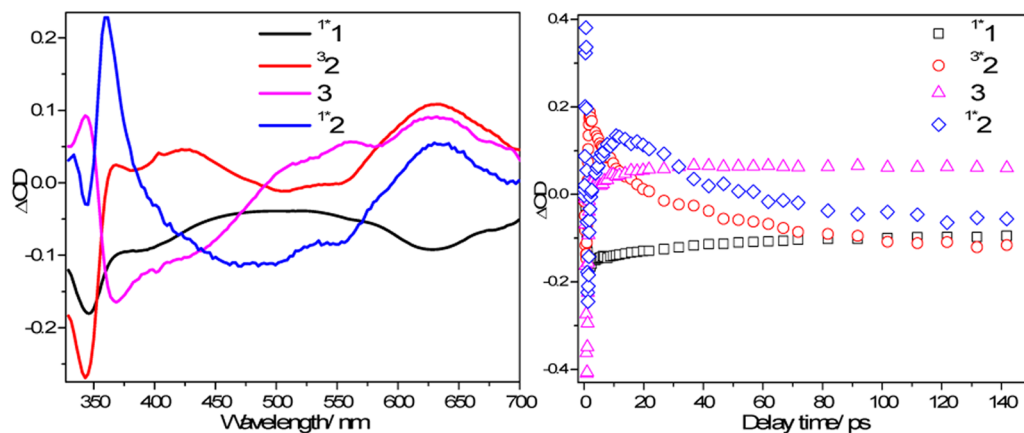

Figure 2. Principal spectra (right) and kinetics (left) of four components obtained by principal components via SVD at the beginning of 150 ps.

In an attempt to confirm how many species were involved after excitation of the photoprecursor **1**, the principal components via singular value decomposition (SVD) method was used to analyze the data obtained at the beginning of 150 ps. The principal components analysis found that there are four components accounting for the evolution spectra at early delay time. Figure 2 displays the principal spectra and kinetics of the first excited singlet state (S_1) of the photoprecursor (^{1*1}), triplet oxenium ion ($^3 2$), open-shell singlet oxenium ion (^{1*2}) and *p*-biphenyloxy radical (**3**).

3.2. Lifetimes for the Observed Transients. In order to obtain the time constant of the different intermediates, a sum of convoluted exponentials function was used to fit a kinetic trace at the selected wavelength, where t_p is instrument response time, t_0 is time zero, A_i and t_i are amplitudes and decay times, respectively. The fitting curve and the residuals are listed in the Supporting Information (SI). Table 1 displays the time constants of the fitting for the selected wavelength.

$$S(t) = e^{-\left(\frac{t-t_0}{t_p}\right)^2} * \sum_i A_i e^{-t-t_0/t_i}$$

Table 1. Shown Are the Time Constants Determined from the Fitting for the Selected Wavelength

wavelength, nm	τ_1, ps	τ_2, ps	τ_3, ps
345	14		
384	4	49	
630	2	42	1613

As mentioned above, the 345 nm transient absorption was assigned to the *p*-biphenyloxy radical, the fitting done for 345 nm found a growth time constant (14 ps) of the *p*-biphenyloxy radical. The *p*-biphenyloxy radical can survive for a long time in acetonitrile (see Figure 1 bottom left). A biexponential function was used to fit the kinetics of 345 nm obtained from the ns-TA spectra and found that a 39 μs time constant could be obtained, which is the lifetime of the *p*-biphenyloxy radical. In contrast, the kinetics of 384 nm could be fitted by a biexponential function, and two time constants can be obtained. The 4 ps is the growth time constant for the generation of the open-shell singlet oxenium ion, while the ~45 ps decay can be associated with the internal conversion (IC) process from the open-shell singlet oxenium ion to the closed-shell singlet oxenium ion, whereas for the kinetics of 630 nm, a triexponential function was required to obtain a best-fit at this wavelength. The 2 ps time constant accounts for the generation of the triplet oxenium ion, the 42 ps time constant is associated with the lifetime of the open-shell singlet oxenium ion, and the 1600 ps time constant is the lifetime of this triplet oxenium ion.

3.3. ns-TR³ Experiments Identify the Long-Lived Transient As the Radical. In the ns-TA spectra a longer-lived transient species has a strong band at 345 nm accompanied by a smaller band at 505 nm (see Figure 1). To learn more about the nature of this longer lived species, we obtained ns-TR³ spectra of it using a 341.5 nm probe wavelength, and this is shown in Figure 3. Time-dependent density functional theory (TD-DFT) computations were done to estimate the transient absorption spectrum for the *p*-biphenyloxy radical, and the comparison between calculated spectrum and experimental spectra is shown in Figure 4; this suggests that the strong 345 nm long-lived band with its weaker
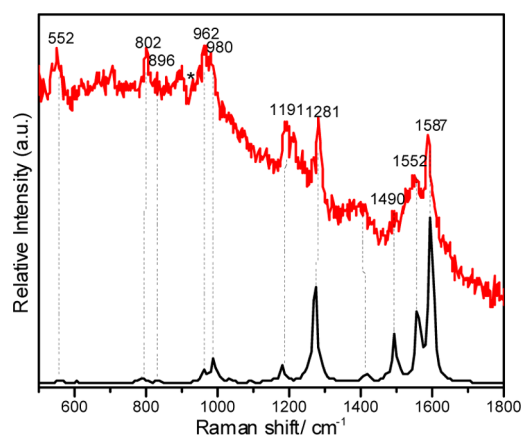
Figure 3. (Top) Ns-TR³ spectrum obtained at 50 ns after 266 nm photoexcitation of **1** and using a 341.5 nm probe wavelength in MeCN. Asterisks represent solvent subtraction artifacts. (Bottom) Calculated normal Raman spectrum of the *p*-biphenyloxy radical (see text for more details).
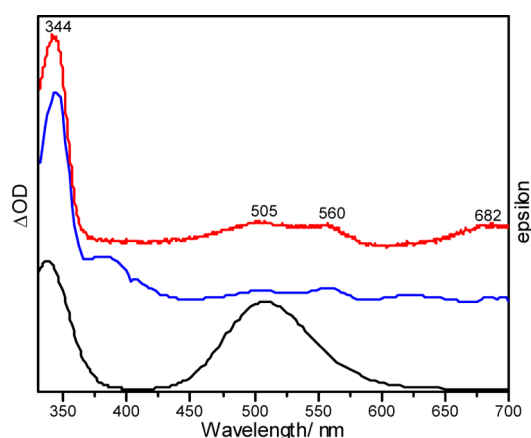
Figure 4. Comparison of the experimental transient absorption spectrum obtained at 400 ns (top) to that obtained at 3022 ps (middle) and with that computed for the UV spectrum (TD-B3LYP/6-311+G(2d,p)) of the *p*-biphenylyl radical (bottom). The top spectrum (red) is assigned to the radical.

505 nm band may be due to the *p*-biphenyloxy radical. The transient absorptions at 560 and 682 nm (see Figure 4) have the same dynamics as that of the transient absorption at 345 nm. Therefore, all of these features on this time scale probably have contributions from the *p*-biphenyloxy radical. DFT calculations were also done to estimate the normal Raman spectrum of the *p*-biphenyloxy radical; this spectrum is shown at the bottom of Figure 3 and compared to the ns-TR³ spectrum obtained using a 341.5 nm probe wavelength at 50 ns after 266 nm photoexcitation of **1** in MeCN that is shown at the top of Figure 3. Inspection of Figure 3 shows that there is excellent agreement between the vibrational frequency patterns of the calculated normal Raman spectrum and the ns-TR³ spectrum obtained at 50 ns. The dotted lines indicate the correspondence of the vibrational features in the calculated and experimental spectra in Figure 3. The preceding results displayed in Figures 3 and 4 led us to assign the relatively long-lived intermediate with a strong peak at 345 nm and a smaller band at 505 nm to the *p*-biphenyloxy radical species. The ns-TA spectra shown in Figure 1 had their kinetic fit, and these data are shown in SI along with a best fit of a

biexponential function that gave decay time constants of $\tau_1 = 39$ μs and $\tau_2 = 258$ μs. The first decay time constant is attributed to the decay of the *p*-biphenyloxy radical to form another species that also has some absorption at 345 nm. The source of the second decay time constant is not yet clear but may be due to some reaction of the radical to form another species, such as the formation of a dimer.

3.4. Assignment of the Other Bands by Time-Dependent Density Functional Theory (TD-DFT) Computations. To help assign the remaining transients, we have performed TD-DFT calculations to estimate the absorption bands for some likely intermediate species that could be generated from the decay of the excited singlet state of **1**. TD-DFT computations have been previously shown to be useful in estimating absorption bands. For example, they are frequently used for assigning absorption bands for carbenes and nitrenes.[34,35] In particular, TD-B3LYP has been used with success to estimate the absorptions of the related ionic intermediates, nitrenium ions.

It is important to consider that oxenium ions can adopt different electronic states. Our computations (Figure 5)

Figure 5. Shown is the TD-DFT calculated relative energies of the closed-shell singlet *p*-biphenylyloxenium ion (S_0), the excited open-shell singlet *p*-biphenylyloxenium ion (S_1), and the triplet *p*-biphenylyloxenium ion (T_1).

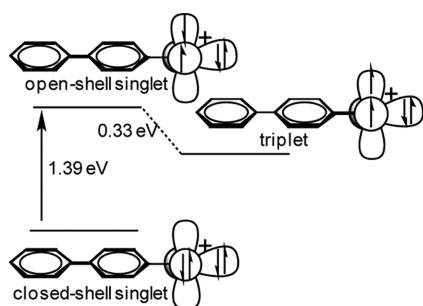indicate that the *p*-biphenylyloxenium ion has a closed-shell singlet ground state with a gap to the lowest energy triplet state of ~24.5 kcal/mol and a vertical gap to the open-shell singlet state of 32 kcal/mol. Thus, unlike many carbenes, it is not possible to see equilibration of singlet and triplet states.

In order to simulate the absorption of the open-shell singlet *p*-biphenylyloxenium ion, TD-DFT was first used to optimize the structure of the open-shell singlet *p*-biphenylyloxenium ion. Then the TD-DFT simulation was performed on the closed-shell state at the open-shell geometry of singlet *p*-biphenylyloxenium ion.[36] Figure 6 (right) displays the comparison of the fs-TA spectrum obtained at a time-delay of 6.8 ps (black line) with the absorption spectra calculated at the (TD-B3LYP/6-311+G(2d,p)) level of theory for the open-shell singlet *p*-biphenylyloxenium ion (blue line) and the triplet *p*-biphenylyloxenium ion (red line). The computed absorption spectrum of the triplet *p*-biphenylyloxenium ion has two bands located at 342 and 621 nm that correspond to the experimentally observed transient absorption bands at 345 and 630 nm. The calculated absorption spectrum of the open-shell singlet *p*-biphenylyloxenium ion has a band located at 384 nm and a shoulder feature centered at 593 nm that corresponds with the experimentally observed transient absorption band located at 394 and 630 nm. These comparisons suggest that both the open-shell singlet and triplet *p*-biphenylyloxenium ion
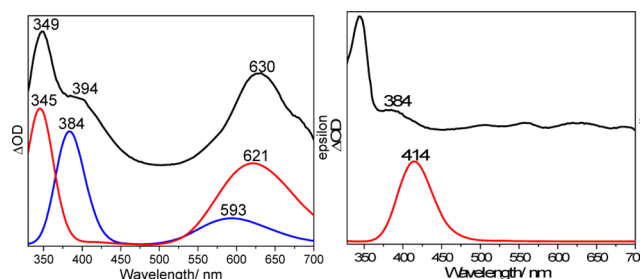
Figure 6. (Right) Comparison of fs-TA experimental spectrum at 6.8 ps with the computed UV spectra (TD-B3LYP/6-311+G(2d,p)) of the excited open-shell singlet *p*-biphenylyloxenium ion (blue) and the triplet *p*-biphenylyloxenium ion (red). (Left) Comparison of fs-TA experimental spectrum at 1222 ps and computed UV spectra (TD-B3LYP/6-311+G(2d,p)) of the closed-shell singlet ground state of *p*-biphenylyloxenium ion.

ions are observed in the fs-TA experiments following 266 nm photoexcitation of **1** in MeCN.

The carrier of the final band at 384 nm is less readily assignable. This transient follows the open-shell singlet *p*-biphenylyloxenium ion and has a time constant of 5−20 ns but is not the open-shell singlet oxenium ion, the triplet oxenium ion, or the radical. Given that all alternative assignments are less plausible, we tentatively assign it to the closed-shell singlet ground state of the oxenium ion. This band also agrees well with the TD-DFT computed spectrum of the closed-shell singlet oxenium ion. That means that the open-shell singlet *p*-biphenylyloxenium ion will undergo an internal conversion process to form the closed-shell singlet *p*-biphenylyloxenium ion. Figure 6 (left) presents the comparison of the fs-TA spectrum obtained at a time-delay of 1222 ps (black line) with the absorption spectra calculated for the closed-shell singlet *p*-biphenylyloxenium ion. This further implies that the 384 nm transient absorption is associated with the closed-shell singlet *p*-biphenylyloxenium ion. TD-DFT computations described above indicate the singlet excited state is ~32 kcal/mol higher in energy than the closed-shell singlet, close to what a recent computational study (CASPT2) found for the energy gap between the open-shell singlet state of phenyloxenium ion and the closed shell configuration (31 kcal/mol).[37] Given that photolysis is performed at 267 nm, each photon carries 107 kcal/mol of radiant energy, and it is certainly energetically plausible that an excited state of ~32 kcal/mol higher in energy than the ground state of the oxenium could be formed. Density functional theory computations (B3LYP/6-31G(d)) find that homolysis of the O−N bond of **1** is uphill by 56 kcal/mol but that heterolysis is essentially isoenergetic with the photoprecursor **1**. Photogeneration of a reactive intermediate excited state is unusual but not without precedent. For example, Platz detected the simultaneous generation of the open-shell singlet and closed-shell singlet fluorenyl carbene upon photolysis of the diazo precursor.[38] Additionally, alternative assignments are less plausible. It is at least in principle possible to observe an S_2 to S_1 conversion of the excited state of **1**, but the carrier of the transient is too long-lived for this possibility to be seriously considered. A more plausible alternative assignment is as an excited T_1 triplet state of the oxenium ion (e.g., a π,π^* triplet oxenium ion), but we view this alternative as less likely given that our computations indicate that the triplet excited state of the photoprecursor is a transition state for forming the n,π^* triplet oxenium ion.

3.5. Product Studies from Photolysis and Thermolysis of 1.
We also hoped to gain insight into the intermediates resulting from the precursor **1** via product studies from thermolysis and photolysis. Table 2 shows the products formed via photolysis and thermolysis under different conditions. Products were identified by comparison to ^{1}H NMR of authentic samples.

Table 2. Product Studies from the Photolysis of Compound 1[a]

Conditions	OH (biphenylol)	OH Cl (chloro adduct)	OH NH3+ (ammonium adduct)	O (water adduct)
Δ CH₃CN	95	5	--	--
Δ H₂O	35	trace	--	65
Δ H₂O 5% NaCl	60	26	5	8
hν CH₃CN	99	trace	--	--
hν H₂O	99	trace	--	--
hν H₂O 5% NaCl	20	80	--	--

[a]Percentages are based on relative ^{1}H NMR integration. Mass balance >78% (see SI for details).

Photolysis in water or acetonitrile gives almost exclusively the reduction product, *p*-biphenylol, with only trace amounts of a chloro trapping adduct. When chloride is added as a trap in water, however, the major product is the chloro adduct, with the reduced product being the minor product. It is possible to envision mechanisms to the reduced product via all the observed intermediates in the photolysis. The radical could form the reduced product via an H atom abstraction, while the oxenium ions could form the reduction product either via a hydride abstraction or via two H atom abstractions followed by a deprotonation. The chloride trapping adduct is clear evidence for an oxenium ion intermediate, as oxenium ions are known to be trapped by nucleophiles at the ortho and para positions of the ring.[4,26,39]

Product studies from thermolysis are similar to those obtained by photolysis. Thermolysis in acetonitrile gives principally the reduced product as seen in the photolysis in acetonitrile. In water, however, the major product is a water trapping adduct at the para position to form a dearomatized product. When the thermolysis is performed in water with added Cl⁻ as a trap, a complex mixture of the reduced product, the ammonium adduct, the chloro adduct, and the water adduct are obtained. A plausible explanation of why water adds to the para position to generate the dearomatized product while chloride and ammonia add to the ortho position could be that para addition is kinetically favored, but reversible. Eventually the aromatized thermodynamic ortho adduct is formed. However, once water is added, a fast deprotonation of the water addition product could render this step irreversible and trap it as the dearomatized product.

4. DISCUSSION AND PHOTOCHEMICAL REACTION SCHEME

Based on the data presented above, the proposed photochemical reaction pathways are shown in Scheme 2. Within 350

Scheme 2. Probable Reaction Pathways and Time Constants for the Open-Shell Singlet *p*-Biphenylyloxenium Ion, the Ground State of the Singlet *p*-Biphenylyloxenium Ion, the Triplet State *p*-Biphenylyloxenium Ion and *p*-Biphenyloxy Radical Are Shown[a]

[a]Note that the triplet excited state of the photoprecursor is computed to be a transition state for a barrierless dissociation of ammonia to give the triplet oxenium ion.

fs, the first excited singlet state is formed of **1**, which partitions into three transients: the *p*-biphenyloxy radical, the open-shell singlet *p*-biphenylyloxenium ion and the triplet *p*-biphenylyloxenium ion. The excited singlet *p*-biphenylyloxenium ion (S_1) state may decay via intersystem crossing (ISC) to the triplet *p*-biphenylyloxenium ion (T_1) species, or via internal conversion (IC) to the ground state of singlet *p*-biphenylyloxenium ion (S_0). In any event, all of the transient species lead to formation of the reduced product, *p*-biphenylol, in the absence of an added trap. Remarkably, in sharp contrast to carbenes and nitrenes, the triplet state of the oxenium ion is shorter-lived than the closed-shell singlet state. For carbenes and nitrenes, usually only the triplet states can be seen with nanosecond spectroscopy, and the singlets have lifetimes on the order of tens of picoseconds. Possibly the shorter-lived triplet is due to the fact that singlet carbenes/nitrenes have a facile C−H insertion pathway and often decay via ISC to lower-energy triplet states. Here, C−H insertion is apparently not an observable reaction channel for singlet oxenium ions, and the triplet is the higher-energy species, making ISC not an energetically favorable decay channel. It is also interesting to speculate that the difference in products between photolysis and thermolysis arise from a change in spin population of the oxenium ion, but more evidence would be needed to verify this claim.

5. CONCLUSION

Using fs-TA, ns-TA, and ns-TR[3] spectroscopic techniques as well as DFT calculations, the present contribution reports an investigation of the photophysical and photochemical reactions of **1** to produce the open-shell singlet *p*-biphenylyloxenium ion, the triplet state *p*-biphenylyloxenium ion, and *p*-biphenyloxy radical intermediates. The properties and kinetics of these

12369

dx.doi.org/10.1021/ja505447q | J. Am. Chem. Soc. 2014, 136, 12364−12370

intriguing reactive intermediates are discussed. This study provides an intriguing demonstration of the importance of excited state dynamics in governing electronic state population of photoprecursors, since the system of Novak and Platz leads to a related closed-shell singlet oxenium ion, whereas the protonated hydroxylamine discussed in this study leads to the radical, the open-shell singlet, and closed-shell singlet states of the oxenium ion and the triplet state of the oxenium ion. To our knowledge, this is the first detection and characterization of a short-lived photochemically generated open-shell singlet or triplet phenyloxenium ion.

■ ASSOCIATED CONTENT

Ⓢ Supporting Information

Compound characterization data, product studies, computational coordinates and absolute energies, kinetic fits, and complete ref 33. This material is available free of charge via the Internet at http://pubs.acs.org.

■ AUTHOR INFORMATION

Corresponding Authors

winter@iastate.edu
phillips@hku.hk

Author Contributions

§M.-D.L. and P.J.H. contributed equally to this work.

Notes

The authors declare no competing financial interest.

■ ACKNOWLEDGMENTS

■ REFERENCES

(1) Peng, H. M.; Webster, R. D. *J. Org. Chem.* **2008**, *73*, 2169.
(2) Olah, G. A., Molnar, A. *Hydrocarbon Chemistry*: John Wiley & Sons: Hoboken, NJ, 2003.
(3) Hanway, P. J.; Winter, A. H. *J. Phys. Chem. A* **2012**, *116*, 9398.
(4) Hanway, P. J.; Xue, J.; Bhattacharjee, U.; Milot, M. J.; Zhu, R.; Phillips, D. L.; Winter, A. H. *J. Am. Chem. Soc.* **2013**, *135*, 9078.
(5) Guerard, K. C.; Chapelle, C.; Giroux, M. A.; Sabot, C.; Beaulieu, M. A.; Achache, N.; Canesi, S. *Org. Lett.* **2009**, *11*, 4756.
(6) Sabot, C.; Guerard, K. C.; Canesi, S. *Chem. Commun.* **2009**, 2941.
(7) Sabot, C.; Commare, B.; Duceppe, M. A.; Nahi, S.; Guerard, K. C.; Canesi, S. *Synlett* **2008**, 3226.
(8) Li, K.-T. *J. Appl. Polym. Sci.* **1994**, *54*, 1339.
(9) Kurti, L.; Herczegh, P.; Visy, J.; Simonyi, M.; Antus, S.; Pelter, A. *J. Chem. Soc., Perkin Trans. 1* **1999**, 379.
(10) Taylor, W. I.; Battersby, A. R. *Oxidative Coupling of Phenols*; Marcel Dekker: New York, 1967.
(11) Baesjou, P. J.; Driessen, W. L.; Challa, G.; Reedijk, J. *J. Am. Chem. Soc.* **1997**, *119*, 12590.
(12) Gamez, P.; Gupta, S.; Reedijk, J. *C.R. Chim.* **2007**, *10*, 295.
(13) Osborne, R. L.; Coggins, M. K.; Raner, G. M.; Walla, M.; Dawson, J. H. *Biochemistry* **2009**, *48*, 4231.
(14) Lewis, J.; Prinn, R. *Planets and Their Atmospheres*; Academic Press: New York, 1994.
(15) Smith, D. *Chem. Rev.* **1992**, *92*, 1473.
(16) Vigalok, A.; Rybtchinski, B.; Gozin, Y.; Koblenz, T. S.; Ben-David, Y.; Rozenberg, H.; Milstein, D. *J. Am. Chem. Soc.* **2003**, *125*, 15692.

(17) Zhang, Y.; Burdzinski, G.; Kubicki, J.; Platz, M. S. *J. Am. Chem. Soc.* **2008**, *130*, 16134.
(18) Wang, J.; Burdzinski, G.; Kubicki, J.; Platz, M. S. *J. Am. Chem. Soc.* **2008**, *130*, 11195.
(19) Winter, A. H.; Gibson, H. H.; Falvey, D. E. *J. Org. Chem.* **2007**, *72*, 8186.
(20) Winter, A. H.; Thomas, S. I.; Kung, A. C.; Falvey, D. E. *Org. Lett.* **2004**, *6*, 4671.
(21) Platz, M. S. *Acc. Chem. Res.* **1995**, *28*, 487.
(22) Siuzdak, G.; North, S.; BelBruno, J. J. *J. Phys. Chem.* **1991**, *95*, 5186.
(23) Hwang, W. G.; Kim, M. S.; Choe, J. C. *J. Phys. Chem.* **1996**, *100*, 9227.
(24) Kosmidis, C.; Ledingham, K. W. D.; Kilic, H. S.; McCanny, T.; Singhal, R. P.; Langley, A. J.; Shaikh, W. *J. Phys. Chem. A* **1997**, *101*, 2264.
(25) Syage, J. A.; Steadman, J. *J. Phys. Chem.* **1992**, *96*, 9606.
(26) Wang, Y. T.; Wang, J.; Platz, M. S.; Novak, M. *J. Am. Chem. Soc.* **2007**, *129*, 14566.
(27) Petrassi, H. M.; Sharpless, K. B.; Kelly, J. W. *Org. Lett.* **2000**, *3*, 139.
(28) Gaucher-Wieczorek, F. S.; Maillard, L. T.; Badet, B.; Durand, P. *J. Comb. Chem.* **2010**, *12*, 655.
(29) Li, M. D.; Ma, J.; Su, T.; Liu, M.; Yu, L.; Phillips, D. L. *J. Phys. Chem. B* **2012**, *116*, 5882.
(30) Chan, P. Y.; Kwok, W. M.; Lam, S. K.; Chiu, P.; Phillips, D. L. *J. Am. Chem. Soc.* **2005**, *127*, 8246.
(31) Li, M. D.; Yeung, C. S.; Guan, X.; Ma, J.; Li, W.; Ma, C.; Phillips, D. L. *Chem.—Eur. J.* **2011**, *17*, 10935.
(32) Scott, A. P.; Radom, L. *J. Phys. Chem.* **1996**, *100*, 16502.
(33) Frisch, M. J.; et al. *Gaussian09*, version A.02; Gaussian Inc.: Pittsburgh, 2009.
(34) Xue, J.; Luk, H. L.; Eswaran, S. V.; Hadad, C. M.; Platz, M. S. *J. Phys. Chem. A* **2012**, *116*, 5325.
(35) Lage, M. L.; Fernandez, I.; Mancheno, M. J.; Sierra, M. A. *Inorg. Chem.* **2008**, *47*, 5253.
(36) Andreu, R.; Garín, J.; Orduna, J. S. *Tetrahedron* **2001**, *57*, 7883.
(37) Hanway, P. J.; Winter, A. H. *J. Am. Chem. Soc.* **2011**, *133*, 5086.
(38) Wang, J.; Kubicki, J.; Hilinski, E. F.; Mecklenburg, S. L.; Gustafson, T. L.; Platz, M. S. *J. Am. Chem. Soc.* **2007**, *129*, 13683.
(39) Novak, M.; Glover, S. A. *J. Am. Chem. Soc.* **2004**, *126*, 7748.